Journal of Marine Research, 66, 61–85, 2008

Critical turbulence revisited: The impact of submesoscale vertical mixing on plankton patchiness

by A. W. Omta[1,2], S. A. L. M. Kooijman[1] and H. A. Dijkstra[3]

ABSTRACT

By supplying nutrients to the ocean surface, submesoscale vertical motions can have a strong impact on phytoplankton growth and phytoplankton distributions. To study this impact, we model a phytoplankton population in a baroclinically unstable submesoscale eddy using a phytoplankton model coupled to a three-dimensional hydrodynamic model. In the eddy, strong vertical transports are generated as a consequence of baroclinic instability. The resulting plankton distributions turn out to depend strongly on the light intensity and local vertical transport. To analyze these distributions in detail, we use more idealized coupled hydrodynamic-biological models and we extend the critical turbulence concept to three dimensions.

1. Introduction

Spatial heterogeneity or 'patchiness' in phytoplankton distributions is ubiquitous in the marine biosphere. Although this phenomenon has been known for a very long time (e.g. Hardy, 1936), there is still a vivid discussion about its causes.

In his excellent review, Martin (2003) discusses the historical development of theories concerning phytoplankton patchiness. The first such theory was the KiSS model formulated independently by Kierstead and Slobodkin (1953) and Skellam (1951). The KiSS model assumes that two processes determine the fate of a phytoplankton patch: biological growth increases the population within the patch and effective horizontal diffusivity causes a population loss from it. According to the model, the population within a patch of constant size will only grow, if the diameter of the patch is larger than a critical value.

After the KiSS model, various explanations for phytoplankton patchiness based on reaction-diffusion models have been put forward. Especially, the Turing (1952) mechanism (e.g. Levin and Segel, 1976; Rothschild and Ault, 1996) and plankton wavefronts (Dubois and Adam, 1976; Petrovskii and Malchow, 1999; Petrovskii, 1999; Petrovskii and Malchow, 2001) have received considerable attention. However, one problem with all these

1. Department of Theoretical Biology, Vrije Universiteit, De Boelelaan 1081, 1081 HV Amsterdam, The Netherlands.
2. Corresponding author. ***email: anne.willem.omta@falw.vu.nl***
3. Institute for Marine and Atmospheric Research Utrecht (IMAU), Universiteit Utrecht, Princetonplein 5, 3582 CC Utrecht, The Netherlands.

models is that they consider horizontal dispersion in the ocean as Fickian diffusion, which means that the features of the flow field are not taken into account. The actual flow field is a crucial factor in some models for the generation of plankton patchiness such as the Lagrangian filament slice model (Tél *et al*., 2005). Consider a patch of phytoplankton surrounded by a region with a high nutrient concentration. On the one hand, the patch will expand in all directions as a consequence of biological growth and diffusion. On the other hand, the strain in the flow will decrease the width and increase the length of the patch. An initially round patch becomes narrower, until the two competing processes (narrowing as a consequence of strain and widening as a consequence of growth) cancel each other. Therefore, this model predicts that patches do not exist below a certain width in nutrient-replete regions. The concept of a minimum width for a phytoplankton filament has already received an observational test. During the SOIREE cruise in the Southern Ocean, a localized phytoplankton bloom was induced by means of iron fertilization (Boyd *et al.*, 2000). The resulting phytoplankton patch was followed in time on color satellite images (Abraham *et al.*, 2000). The patch's length increased over the course of the experiment, whereas its width stabilized at 4 km, suggesting that there indeed exists a minimum width of plankton filaments in the sea.

Observations often show quite similar slopes of Fourier spectra of plankton and of 'inert' tracers (temperature, salinity) across a large range of scales (from $O(10\text{ m})$–$O(100\text{ km})$ (Smith *et al.*, 1988; Seuront *et al.*, 1996, 1999). The usual interpretation is that within this range the two-dimensional turbulent stirring dominates biological effects and is solely responsible for the phytoplankton spatial distribution. However, it is unlikely that horizontal stirring generates patchiness on its own accord. Probably, there is always a 'seed' heterogeneity which may come from purely biological effects such as predator-prey interactions or from localized upwelling of nutrients triggering phytoplankton growth. Strong upwelling particularly occurs at the (sub-)mesoscale in regions with frontal dynamics. Strass (1992) has described observations of a mesoscale front where upwelling induced large amplitude, localized blooms of phytoplankton. This led to a flattening of the chlorophyll spectrum at scales of 15–35 km, whereas the spectrum had approximately the same slope as the spectrum of salinity at smaller and larger scales.

Flierl and McGillicuddy (2002) have given an extensive overview of physical mechanisms that can generate upwelling at the (sub)mesoscale. Baroclinic Rossby waves, single propagating eddies (McGillicuddy *et al.*, 1995, 1998), interaction of multiple eddies (McGillicuddy and Robinson, 1997), jet meandering (Woods, 1988; Flierl and Davis, 1993), baroclinic instability (Charney, 1947; Eady, 1949) and (sub)mesoscale Ekman flow (Stern, 1965; Niiler, 1969) can all give rise to significant vertical transports.

Given that upwelling can supply the nutrients necessary for the generation of phytoplankton blooms, one may expect that patches of high phytoplankton are generally found at upwelling locations. However, simulations (Spall and Richards, 2000; Omta *et al.*, 2007) indicate that this does not need to be the case (even in an oligotrophic region). In these simulations, vertical transports do promote plankton growth by supplying nutrients from the

deep sea, but the highest plankton concentrations are not always found at actual upwelling sites. Upwelling brings water parcels with a high nutrient concentration, but with a low phytoplankton concentration to the surface. To consume the upwelled nutrients and to multiply, algae need time during which the water parcels can be transported quite far from the actual upwelling location.

The relationship between upwelling and plankton patch formation is further complicated by the fact that vertical transports will only stimulate phytoplankton growth as long as the organisms are nutrient-limited; if the organisms are light-limited, they are not able to utilize the upwelling nutrients for growth. Whether the algae are light-limited is probably not only dependent on the surface light intensity, but also on the vertical water exchange. According to the classical Sverdrup (1953) critical-depth theory, phytoplankton can become light-limited, if the mixing layer is too deep. Furthermore, simulations and theory by Huisman *et al.* (1999) of a plankton community in a one-dimensional water column suggest the existence of a so-called 'critical turbulence.' If the vertical mixing exceeds these critical conditions, then plankton is mixed out of the euphotic zone before it has had the opportunity to grow and therefore, the population will go extinct. However, if the vertical mixing is very low, then the plankton will become strongly nutrient-limited which leads to a low equilibrium plankton concentration. Between these two extremes, there appears to exist an optimal vertical mixing regime where the phytoplankton is neither strongly light- nor strongly nutrient-limited.

The critical depth and critical turbulence concepts were based on a one-dimensional picture of algae living in a water column, with vertical transports provided by constant Fickian diffusion. This view is of course a gross simplification of dispersion in the real ocean which occurs in three-dimensional, time-dependent flows. Nevertheless, nutrient- and light-limitation do exist, regardless of the specifics of the flow, and they can probably play a distinct role in patch formation in three dimensions. Furthermore, vertical water exchange will have an impact on nutrient and light limitation in three dimensions as well. In this paper, we investigate this impact by simulating a phytoplankton community in a relatively simple submesoscale flow situation of a single initially cyclo-geostrophic eddy that is baroclinically unstable. An important advantage of this flow over a baroclinically unstable jet generating a field of transient eddies as in e.g. Lévy *et al.* (2001, 2003) is that the developing vertical velocity field is dominated by a relatively simple flow structure. This makes it much easier to entangle causes and effects. We will show that in these three-dimensional flows, the existence of a local critical level of vertical exchange or a critical light intensity is responsible for the spatial distributions of the plankton.

2. Models and methods

We consider a horizontally square ocean domain of length $L = 32$ km with a constant depth H of 1 km and use Cartesian coordinates x, y and z, with $z = -H$ at the bottom and $z = 0$ at the surface. The domain is located on an f-plane with fixed Coriolis parameter $f_0 = 10^{-4}$ s^{-1}. The stratification of the ocean water in this domain is only determined by

the temperature T. For $t < 0$ the ocean water is motionless and stably stratified according to a temperature distribution

$$T_b(z) = T_0 + T_1 e^{\frac{z}{z_b}} \tag{1}$$

where z_b is the vertical temperature decay depth ($z_b > 0$). In this way, the vertical temperature difference between top and bottom is given by $\Delta T = T_1(1 - e^{-\frac{H}{z_b}})$. A sub-mesoscale eddy is introduced at $t = 0$ by an imposed temperature anomaly as described in more detail below.

To model the phytoplankton, we use the SU-based Internal Transformation Yield (SITY) model that can be considered as a simplification of the earlier mixotroph (Kooijman *et al.*, 2002) and PINC (Omta *et al.*, 2006, 2007) models. However, contrary to these earlier models, no maintenance and reserves are included. Following the DEB convention (Kooijman, 2000), we denote concentrations of compounds with the letter X, i.e. X_N for the nutrient concentration, X_V for the concentration of living biomass, and X_D for the detritus concentration. In this way, it is straightforward to see which symbols denote concentrations and what their physical dimensions are. Our model accounts for multiple nutrient limitation by using a Synthesising Unit (SU) transformation (Kooijman, 2000) for biological uptake and growth according to:

$$\mu = \frac{\mu_{max}}{1 + x_N^{-1} + x_L^{-1} - (x_N + x_L)^{-1}}, \quad x_N = \frac{X_N}{K_N}, x_L = \frac{J_{L,F}}{J_{L,FK}}, \tag{2}$$

where μ denotes the growth rate, μ_{max} the maximum growth rate, K_N the nutrient half-saturation concentration, $J_{L,F}$ the external light intensity, and $J_{L,FK}$ the half-saturation light intensity. The quantities x_N and x_L can be thought of as scaled availability of nutrient and light, respectively. The light flux $J_{L,F}$ (in mol/(m^{2}d)) as a function of the vertical coordinate z is prescribed as:

$$J_{L,F} = J_{L,S} e^{\frac{z}{d}} \tag{3}$$

with an attenuation depth d (and z going negative with depth).

Mortality is implemented using a constant rate h_V at which biomass (X_V) turns into detritus (X_D). To close the nutrient cycle, we impose a simple constant rate h_D at which detritus (X_D) turns into nutrient (X_N). This can be interpreted as remineralization of detritus by some constant background population of bacteria. The biological model is now given by

$$\frac{dX_N}{dt} = -\mu X_V + h_D X_D \tag{4a}$$

$$\frac{dX_V}{dt} = (\mu - h_V) X_V \tag{4b}$$

$$\frac{dX_D}{dt} = h_V X_V - h_D X_D \tag{4c}$$

where the standard values of the parameters are given in Table 1.

Table 1. Model parameter values; the dashed line separates the parameters of the plankton model from the parameters of the flow model.

Parameter	Interpretation	Units	Value
μ_{max}	Max. growth rate	d^{-1}	2.5
K_N	Sat. const. nutrient uptake	μM	0.1
$J_{L,FK}$	Sat. light flux	mol/(m^2d)	25
$J_{L,S}$	Surface light intensity	mol/(m^2d)	50
d	Attenuation depth	m	14
h_V	Death rate	d^{-1}	0.1
h_D	Detritus decay rate	d^{-1}	0.1
w_S	Detritus sinking speed	m/d	10
ρ_0	Background water density	kg/m^3	10^3
f_0	Coriolis parameter	s^{-1}	10^{-4}
T_0	water temperature at infinite depth	°C	5
$T_0 + T_1$	background surface water temperature	°C	8
ΔT	characteristic vertical temperature difference	°C	3
α_T	thermal water expansion coefficient	$°C^{-1}$	10^{-5}
g	acceleration due to gravity	m/s^2	10
D_H	horizontal mixing coefficient	m^2/s	0.1
D_V	vertical mixing coefficient	m^2/s	10^{-5}
z_b	background vertical temperature decay depth	km	0.4
z_e	eddy decay depth	km	0.25
ΔT_e	maximum eddy temperature disturbance	°C	1.8
r_0	initial eddy radius	km	4

The flow model is nonhydrostatic; its numerical details are described in Molemaker and Dijkstra (2000). The coupling of this model with plankton models in the case of an eddy flow is described in Omta *et al.* (2007). The equations describing the flow development and the changes in the phytoplankton population density are given by

$$\frac{\partial \mathbf{u}}{\partial t} + (\mathbf{u}\cdot\nabla)\mathbf{u} + f_0\mathbf{e_z}\times\mathbf{u} = -\frac{1}{\rho_0}\nabla p + D_H\left(\frac{\partial^2}{\partial x^2}+\frac{\partial^2}{\partial y^2}\right)\mathbf{u} + D_V\frac{\partial^2\mathbf{u}}{\partial z^2} - \mathbf{e_z}\frac{g\rho}{\rho_0} \tag{5a}$$

$$\nabla\cdot\mathbf{u} = 0 \tag{5b}$$

$$\frac{\partial T}{\partial t} + (\mathbf{u}\cdot\nabla)T = D_H\left(\frac{\partial^2}{\partial x^2}+\frac{\partial^2}{\partial y^2}\right)T + D_V\frac{\partial^2 T}{\partial z^2} \tag{5c}$$

$$\frac{\partial X_i}{\partial t} + (\mathbf{u}\cdot\nabla)X_i + w_S\delta_{i3}\frac{\partial X_i}{\partial z} =$$

$$D_H \left(\frac{\partial^2}{\partial x^2} + \frac{\partial^2}{\partial y^2} \right) X_i + D_V \frac{\partial^2 X_i}{\partial z^2} + F_i, i = 1, 2, 3 \tag{5d}$$

$$\rho = \rho_0 (1 - \alpha_T (T - T_0)) \tag{5e}$$

where the last equation expresses that a linear equation of state is used; here T_0 and ρ_0 are reference values of temperature and density, respectively. In these equations, the quantities D_H and D_V are the constant horizontal and vertical mixing coefficients of momentum and tracers. The biological fluxes F_i, $i = 1, 2, 3$ for the quantities $X_i \in \{X_N, X_V, X_D\}$ are the right-hand sides of the Eqs. 4a through 4c. In Eq. (5d), the quantity w_S is the vertical sinking velocity of detritus and δ_{ij} is the Kronecker symbol.

We assume periodic boundary conditions in the horizontal for all quantities. In the vertical, we assume slip conditions for the flow field and no-flux conditions for the quantities T, X_N, X_V and X_D. The initial vertical distribution of the biological tracers (determined from a simulation with the model under no-flow conditions) is in equilibrium: the downward sinking flux of detritus is cancelled by an upward diffusive flux of inorganic nutrient. The vertical profiles of X_N, X_V and X_D are plotted in Figure 1a-c, respectively, and show the typical surface depletion of nutrients and the subsurface maxima of biomass and detritus. The initial flow conditions are the same as in Omta *et al.* (2007); the initial eddy is introduced by a temperature anomaly

$$T_e(r, z) = -\Delta T_e e^{-\left(\frac{r}{r_0}\right)^6} e^{\frac{z}{z_e}} \tag{6}$$

where $r = ((x - L/2)^2 + (y - L/2)^2)^{1/2}$ is the distance from the center of the domain, ΔT_e is the maximum temperature difference between the background temperature distribution and the center of the eddy, r_0 is the horizontal eddy radius, and z_e defines the vertical decay scale. The accompanying velocity field is in cyclo-geostrophic equilibrium; this flow field was determined analytically. A vector plot of the horizontal velocity field just below the surface is shown in Figure 1d. The eddy is rotating counterclockwise and typical horizontal velocities are in the order of 5 cm/s.

The equations for the biological quantities require a sophisticated advection scheme to prevent the occurrence of negative concentrations. As in Omta *et al.* (2007), we have used a third-order upwind scheme with limiter (Hundsdorfer and Verwer, 2003) for the advection of the biological tracers. This scheme guarantees positive definite advection.

3. Results

We have run the coupled hydrodynamic-biological model at a horizontal resolution of 160 m and a vertical resolution of 20 m (a grid of $200 \times 200 \times 50$) with a timestep of 75 seconds over a time interval of about 12 days.

As in Legg *et al.* (1998); Noh *et al.* (2003); Drijfhout (2003), baroclinic instability leads to the formation of sub-structures and the eventual break-up of the eddy. More specifically,

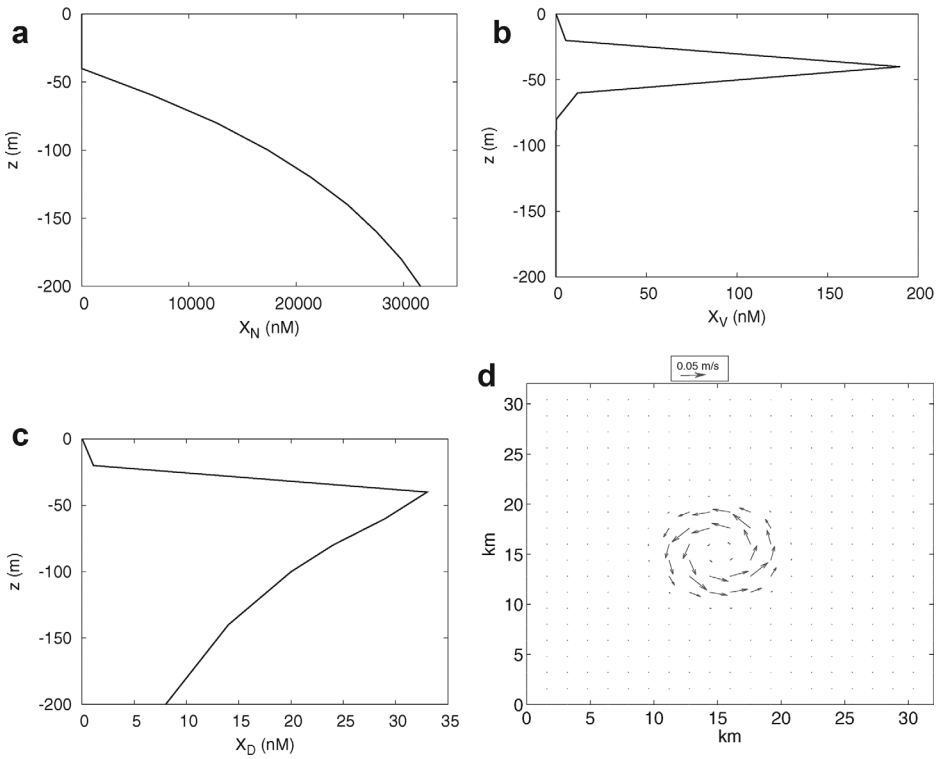

Figure 1. Initial conditions of the simulation. Vertical profiles throughout the upper 200 m of the domain of (a) X_N, (b) X_V and (c) X_D and (d) Vector plot of the initial horizontal velocity distribution of the eddy 50 m below the surface. The amplitude of this velocity field decays with depth and the initial vertical velocity is equal to zero everywhere.

the baroclinic instability results in an azimuthal wavenumber $m = 4$ pattern (the most unstable eigenmode). Such a four-lobe flow pattern has become obvious in the vertical velocity field (w) after 3.6 days (Fig. 2a). At this point in time, the downward velocities have been organized along remarkable spiral structures. The width of these spirals is about 1 km and the distance between the arms is a few kilometers. Between the spirals, there are regions with upward vertical motion. Superimposed on the four-lobe structure, smaller-scale structures can be seen. The four anomalies rotate counterclockward and move away from the eddy centre. After 7.2 days, they have started to separate themselves from the parent eddy, which is clearly visible in the spatial pattern of w in Figure 2b. After 12 days, the inner eddy appears to undergo again an instability associated with an $m = 4$ mode, while the lobes seem to become unstable to an $m = 2$ mode (Fig. 2c). By this time, the lobes have moved nearly to the boundary of the domain; they may start to be affected by their mirror images because of the periodic boundary conditions. Therefore, we have ended the simulation at this point.

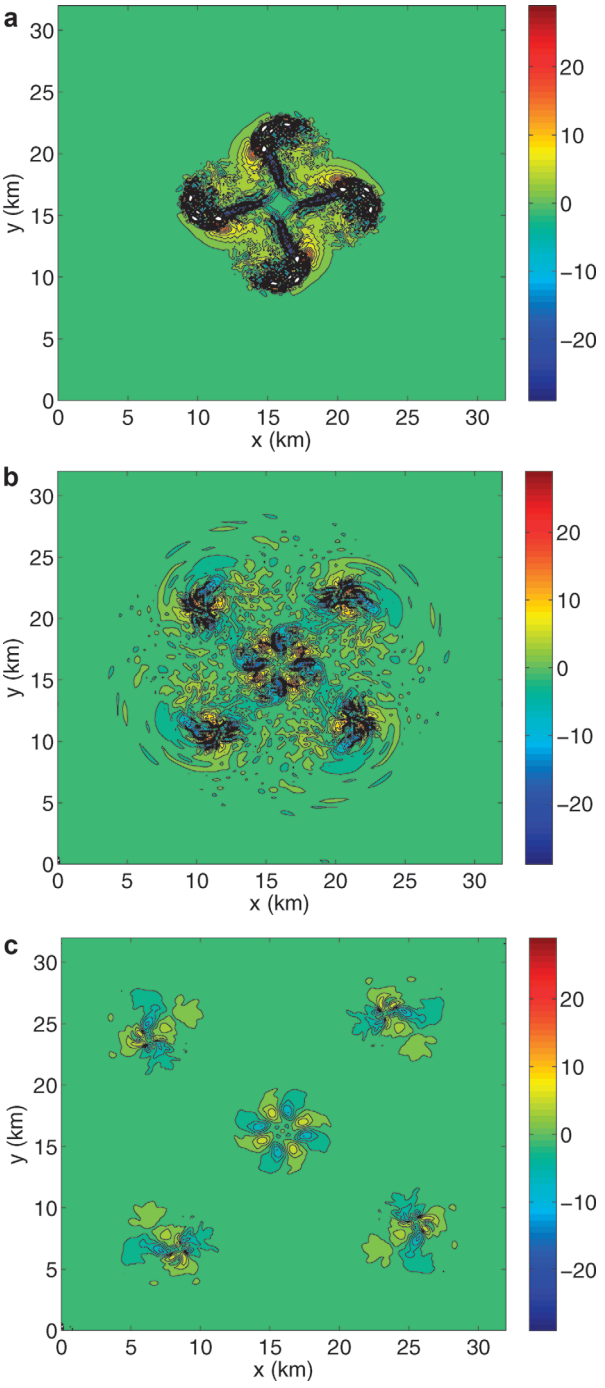

Figure 2. Horizontal cross-sections of the vertical velocity at 20 m depth after (a) 3.6 days, (b) 7.2 days, and (c) 12 days. Values are in 10^{-4} m/s.

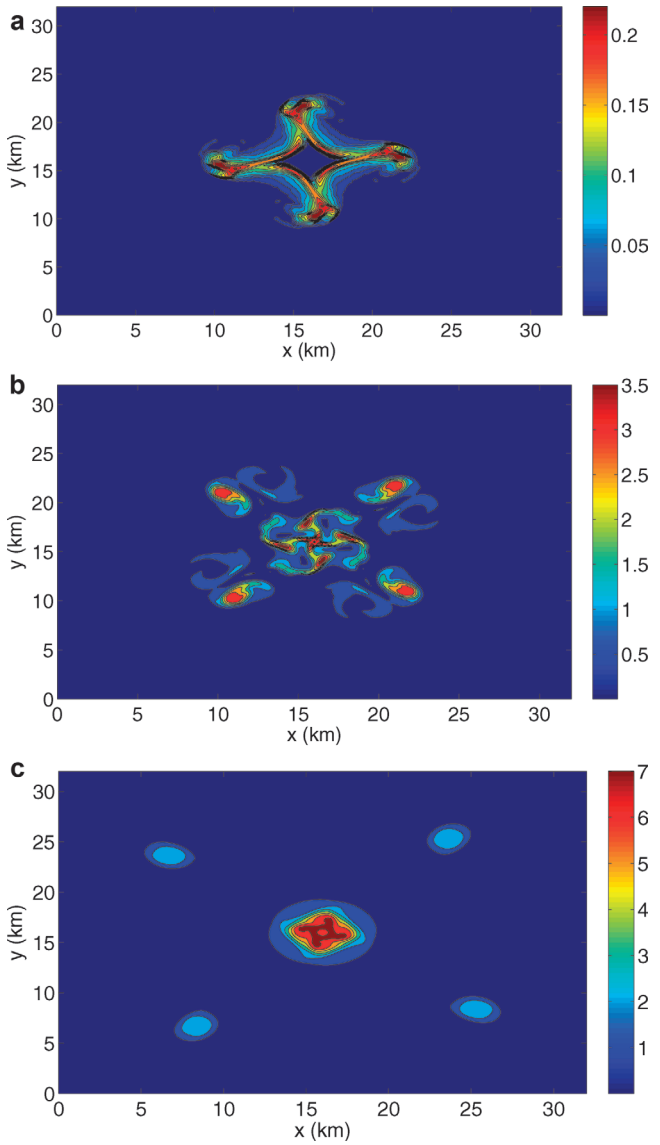

Figure 3. Horizontal biomass patterns (X_V) at the surface at various times for Case A ($J_{L,S} = 50$ mol(m^{2}d) and $d = 14$ m). Values are in μM (note change in color scale between panels). (a) After 3.6 days (b) After 7.2 days (c) After 12 days.

For the standard model parameter values (given in Table 1), the surface distribution patterns for X_V at various times are shown in Figure 3. The temporal development of these patterns shows some marked details. At first, the vertical advective exchange is largest in the spokes connecting the eddies and the lobes (see Fig. 2a), leading to upward nutrient

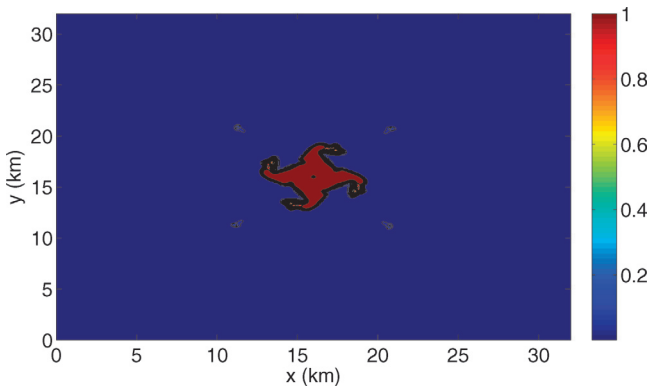

Figure 4. Horizontal nutrient pattern (X_N) at the surface after 7.2 days for Case A ($J_{L,S} = 50$ mol/(m^{2}d) and $d = 14$ m). Values are in μM.

transport and an initial bloom in these areas (see Fig. 3a). After 7.2 days, the lobes have separated themselves from the central eddy (see Fig. 2b) and the vertical exchange is largest within the parent eddy and the four separated features. Therefore, the bloom develops further in those regions, whereas it has already declined in the other areas. Between 7.2 and 12 days, the bloom continues in the interior patch, whereas the plankton concentration declines in the outer features during this period. This dichotomy can be understood by considering the surface nutrient distribution after 7.2 days: the nutrient concentration is still very high (above 1 μM) in the central patch, whereas the nutrients have already largely been depleted in the outer features (see Fig. 4). Another interesting detail is the 'smearing out' of the plankton distribution between 7.2 and 12 days. Probably, this is mainly caused by horizontal diffusion as the horizontal diffusion length scale for this period of 4.8 days (4.0×10^5 s) is approximately equal to $\sqrt{D_H t} = \sqrt{0.1 \times 4.0 \times 10^5} = 200$ m.

To investigate the impact of light conditions on the biomass distributions, we performed simulations at various light arrival fluxes ($J_{L,S}$) of 50 (the standard simulation), 5, and 2 mol/(m^{2}d) at the surface. We have defined these simulations as cases A, B, and C, respectively; in Table 2, the values of $J_{L,S}$ are summarised for the different cases. In Table 3, we

Table 2. Summary of the surface light intensity $J_{L,S}$ and the attenuation depth d for the different three-dimensional simulations. We have also included the resulting critical turbulence D_{Vc}, determined from one-dimensional water column simulations.

		$J_{L,S}$ (mol/(m^{2}d))	d (m)	D_{Vc} (m^2/s)
Case	A	50	14	0.35
	B	5	14	0.009
	C	2	14	0.001
	D	5	7	0.006

Table 3. Maximum biomass concentrations $X_{V,max}$ in μM at the different transects of Figure 5.

		Case			
		A	B	C	D
Time (d)	3.6	0.2	0.1	0.2	0.3
	7.2	3.5	0.1	0.2	0.4
	12	7.2	0.7	0.3	1.6

show the maximum surface biomass concentrations for each of the simulations at different times. The highest biomass concentrations are reached in the (standard) Case A, whereas Case C yields the lowest biomass concentrations of the different simulations. In Figure 5, we show horizontal one-dimensional transects of X_V at the upper surface of the domain at different times and in Figure 6 we show two-dimensional surface distribution patterns after 12 days. In Case A, the highest biomass concentrations are found within the eddy and in the lobes, whereas the maximum concentration is in the regions surrounding the eddy and

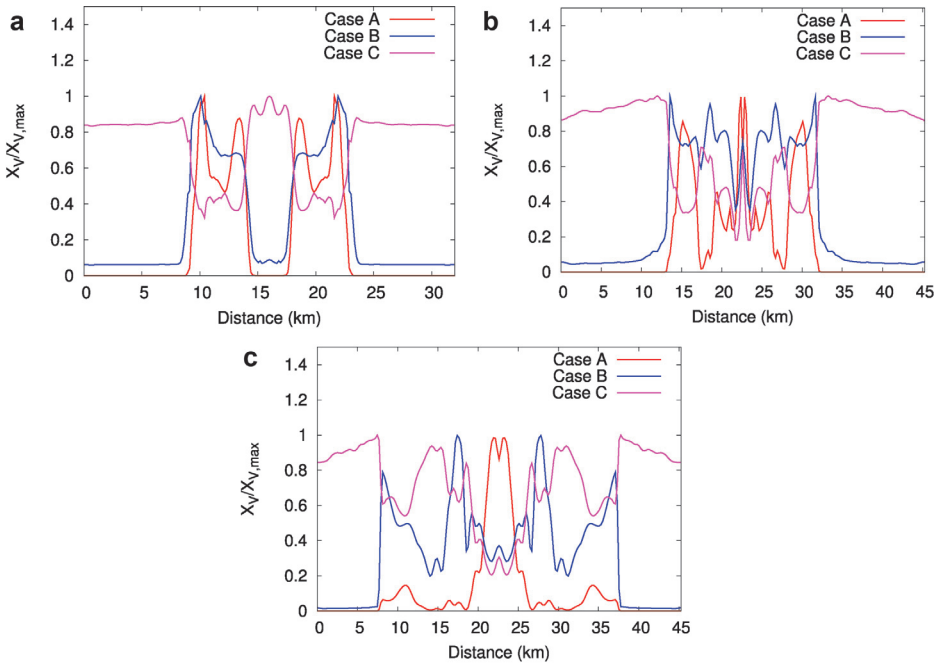

Figure 5. Sections of scaled surface biomass concentrations at different times under various light conditions. Values of the maximum biomass concentration $X_{V,max}$ are given in Table 3. Because of the location of the lobes, the section was taken from south to north through the centre of the eddy after 3.6 days, whereas the section was taken from southwest to northeast through the centre of the eddy after 7.2 and 12 days. (a) After 3.6 days (b) After 7.2 days (c) After 12 days.

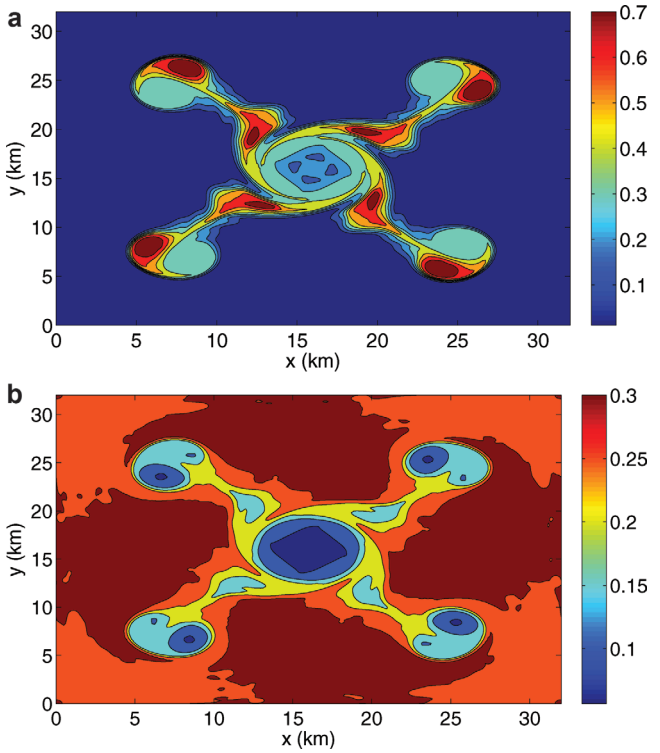

Figure 6. Horizontal biomass patterns (X_V) at the surface after 12 days. Values are in μM (note change in color scale between panels). (a) Case B ($J_{L,S} = 5$ mol/(m^{2}d) and $d = 14$ m) (b) Case C ($J_{L,S} = 2$ mol/(m^{2}d) and $d = 14$ m).

the lobes in Case C. In Case B, the highest concentrations are found in the lobes and at the edge of the eddy.

To gain further insight into the relationship between light limitation and plankton distributions, we performed simulation D where the effects were expected to be enhanced. In this simulation, we used a shorter attenuation depth d (7 m instead of 14 m), with $J_{L,S} = 5$ mol/(m^{2}d). This shorter attenuation depth implied a thinner euphotic zone. Therefore, we expect a relatively strong impact of light limitation in the regions with vigorous vertical exchange. On the other hand, the growth rate of plankton that stays on the surface (i.e., plankton in regions with a low vertical exchange) is independent of the attenuation depth and hence, we expect the influence of light limitation to be relatively low in regions without strong vertical exchange.

In Figure 7, we show two-dimensional surface biomass distribution patterns for Case D after 7.2 and 12 days. After 7.2 days, the highest biomass concentrations are found outside the eddy and the lobes, whereas they are found within the lobes after 12 days. The

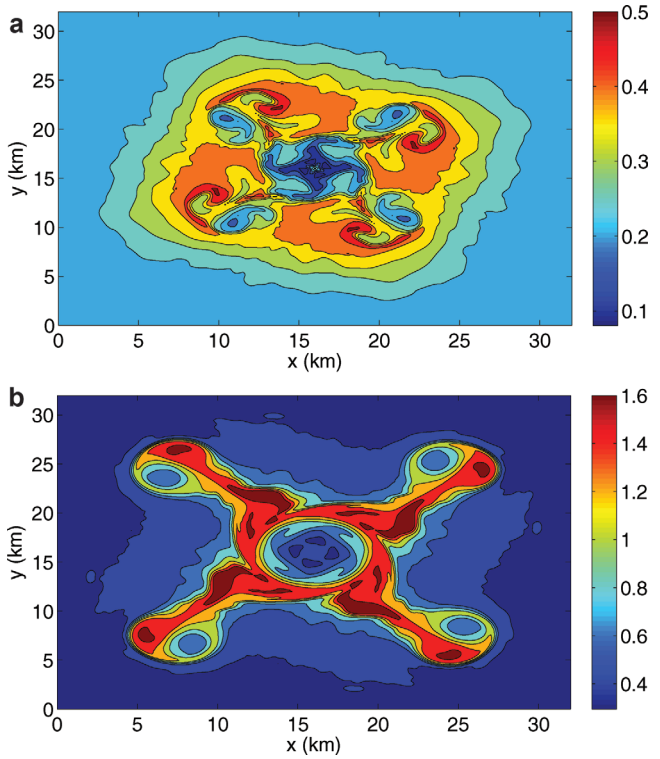

Figure 7. Horizontal biomass patterns (X_V) at the surface for Case D. Values are in μM (note change in color scale between panels). (a) After 7.2 days (b) After 12 days.

maximum surface biomass concentrations (Table 3) are slightly higher than in the Cases B and C, but much lower than in Case A. In the eddy core, the plankton growth seems to be inhibited all the time; in the lobes, the plankton growth seems to be inhibited at first, whereas the organisms in that region achieve very high growth rates during the later part of the simulation. In Section 4, we will explain these findings as a consequence of a change in the vertical exchange conditions during the simulation.

4. Analysis

To understand the results in the previous section in more detail, we used a two-dimensional (one horizontal and one vertical dimension) model in which the relevant transport processes are modelled in a very simplified manner. There exists no advection in this 2D model, all the horizontal and vertical exchange is modelled using (eddy) diffusivities. In the 3D-hydrodynamic simulations, there exists an eddy region with a large vertical exchange and a surrounding region with a low vertical exchange. In our 2D simulations, we mimicked this

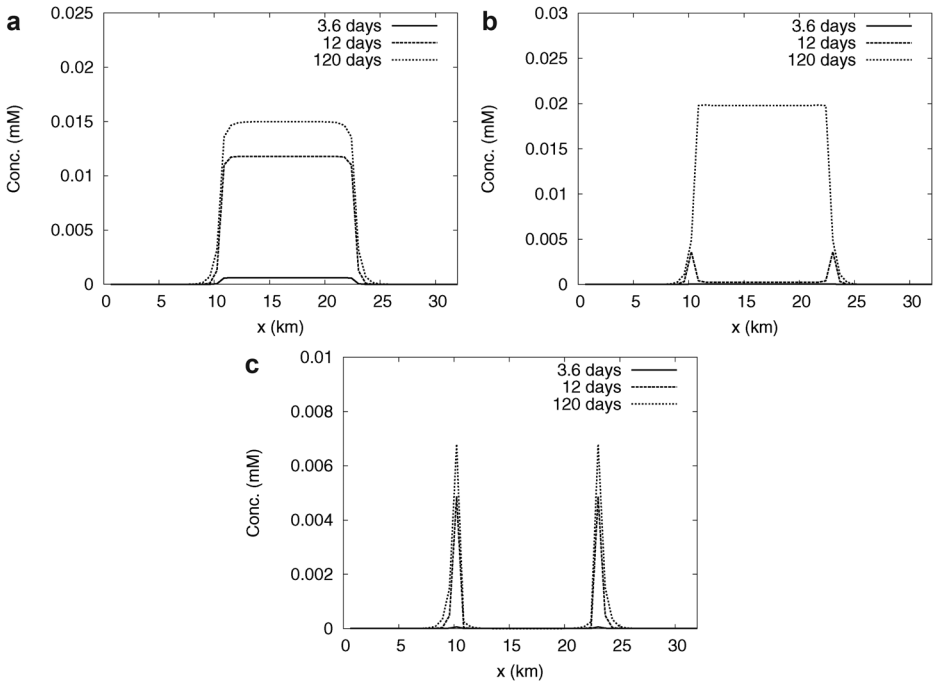

Figure 8. Surface biomass concentrations after different times from the 2D model for Case A ($J_{L,S} =$ 50 mol/(m^{2}d), $d = 14$ m). (a) Vertical mixing in 'eddy region' $D_V = 0.01$ m^2/s (b) Vertical mixing in 'eddy region' $D_V = 0.1$ m^2/s (c) Vertical mixing in 'eddy region' $D_V = 1$ m^2/s.

situation by defining an 'eddy region' with a high vertical diffusion surrounded by a 'non-eddy region' with a constant low vertical diffusion of $D_V = 1.0 \times 10^{-5}$ m^2/s. The domain was 32 km wide in the horizontal and 1 km deep in the vertical; the horizontal resolution was 640 m, while the vertical resolution was 20 m, with the 'eddy region' for 10 km $< x <$ 22 km and the 'non-eddy region' throughout the rest of the domain. The horizontal diffusivity $D_H = 0.1$ m^2/s everywhere in the domain. We imposed periodic boundary conditions in the horizontal and no-flux boundary conditions in the vertical. Because these 2D simulations took much less time than the 3D runs, we were able to run the simulations until the plankton population had approached equilibrium after 120 days.

First, we have varied the vertical diffusivity in the eddy region for Case A ($J_{L,S} =$ 50 mol/(m^{2}d) and $d = 14$ m). It turns out that two regimes exist: if $D_V < 0.35$ m^2/s, then the highest biomass concentrations eventually appear in the 'eddy' region; if $D_V >$ 0.35 m^2/s, then the highest biomass concentrations appear in narrow strips just outside the 'eddy region' (see Fig. 8). Subsequently, we have performed the same experiment for Case C ($J_{L,S} = 2$ mol/(m^{2}d) and $d = 14$ m). Again, we found a regime with the highest biomass

concentrations in the 'eddy region' and another regime with the highest biomass concentrations just outside that region. In this experiment, however, the boundary between the two regimes was at a much lower vertical diffusivity in the 'eddy region': $D_{Vc} = 0.001$ m^2/s.

To gain a better understanding, we have also performed simulations of the plankton population in a one-dimensional water column with the parameter values of each of the four cases. By varying the vertical mixing D_V, we determined D_{Vc}, i.e. the critical turbulence as proposed by Huisman *et al.* (1999); it defines the vertical mixing above which there is no net growth of plankton. It turns out that for each of the cases, D_{Vc} (see Table 2) coincides with the boundary between the two regimes in the two-dimensional simulations.

Using the critical turbulence concept, the regimes can be understood as follows: if the vertical mixing in the 'eddy region' is below the critical value, then the strong mixing stimulates plankton growth by supplying nutrients to the euphotic zone, leading to a bloom in that region. If the vertical mixing in the 'eddy region' exceeds the critical value, then the mixing still supplies nutrients to the euphotic zone. However, there does not emerge a plankton bloom, because the rate at which plankton is transported downward out of the euphotic zone is larger than the maximum biological growth rate. Nevertheless, horizontal diffusion transports nutrients from the 'eddy' region to the areas adjacent to the region of high mixing. In these areas, the conditions for plankton growth are optimal: a high nutrient concentration and a low vertical mixing (i.e. no severe light limitation).

In general, the (transient) distributions after 12 days look qualitatively the same as the (near-equilibrium) distributions after 120 days. However, if the vertical mixing in the eddy region is close to D_{Vc}, then the shape of the distribution after 12 days is different from the shape of the distribution after 120 days in some cases. An example is provided by Figure 8b. Here, the highest biomass concentration is just outside the eddy after 12 days, whereas it is inside the eddy after 120 days. This qualitative change in time can be understood roughly by considering the growth and loss rates of biomass in the different regions. At every point in time, the loss rate is larger within the eddy, because of the larger vertical mixing. The growth rate is practically the same inside and just outside the eddy for some time because the plankton growth is nutrient-saturated, but once the plankton population has largely depleted the nutrients, it becomes much larger inside the eddy than outside. For this reason, the net growth (growth minus loss) is at first smaller inside the eddy than in the adjacent region, but later, the net growth becomes largest inside the eddy. Eventually, the biomass concentration at the edges is overtaken by the biomass inside the eddy.

Although the 2D model is a substantial simplification of the 3D hydrodynamic-biological model, the resulting biomass distributions share important characteristics. In both model simulations, two regimes can be distinguished: one with the highest biomass concentrations in the eddy, the other with the highest biomass concentrations just outside the eddy. This suggests that these different regimes can be understood in essentially the same way in both model setups, even though different transport mechanisms (i.e. advection versus diffusion) are at work. Therefore, we will draw analogies between the 2D and the 3D results and we will explain the main patterns in the 3D model simulations using the critical turbulence

Table 4. Vertical flux (advection + diffusion) of living biomass (X_V) across the base of the euphotic zone and biological population growth within the euphotic zone in the region 15 km $< x <$ 17 km, 15 km $< y <$ 17 km at different times for the Cases A and C. Values are in mmol/(m^{2}d). The base of the euphotic zone is taken at 70 m depth for Case A and at a depth of 30 m for Case C. Positive values imply an upward flux of biomass or a net biological population growth.

		Case A		Case C	
		Vert. flux	Growth	Vert. flux	Growth
Time (d)	3.6	−0.094	11.746	−0.453	0.313
	7.2	−0.049	118.023	−0.131	0.083
	12	0.008	279.567	−0.005	0.098

concept. As in the 2D model simulations, there exists vertical exchange leading to an upward transport of nutrients and a downward transport of biomass. The upward transport of nutrients fuels plankton growth at the surface. If this growth is larger than the downward transport of biomass, then the population will increase; if the downward transport of biomass is larger than the growth, then the population will decrease. Furthermore, in both the 3D and the 2D simulations, the vertical exchange is much larger in the center (eddy) region than in the outer areas. Depending on the vertical exchange and the light conditions, either the plankton growth 'wins' in the eddy region, leading to a biomass maximum within the eddy, or the downward transport of plankton 'wins', leading to low biomass in the eddy region. In Table 4, we compare the downward transport of biomass with the biological population growth in the central region of the eddy for the 3D simulations Case A and Case C. In Case A, the growth 'wins': it is much larger than the downward transport, whereas in Case C, the downward transport 'wins': it is larger than the growth, except after 12 days (when the vertical flow velocities have already strongly decreased). In both the 2D and 3D cases, horizontal exchange generates nutrient transport from the eddy region to the areas adjacent to the eddy, fueling a relatively high plankton growth in these adjacent regions. However, calculations of the actual fluxes show that in the 3D case, there exists an even larger vertical transport of nutrients towards the areas adjacent to the eddy. If the biomass inside the eddy is low, the relatively high nutrient concentration in the adjacent regions can lead to a biomass maximum outside the eddy. Hence, the combined effect of light limitation and vertical and horizontal nutrient transports can lead to the formation of strips with a relatively high biomass concentration around the eddy and the lobes. On the other hand, if the vertical exchange does not exceed the critical value in the eddy and the lobes, then the highest biomass concentrations are found within the eddy and the lobes.

In the simulations with the 3D model, we also noticed situations which do not clearly fall into either one of the two specific regimes. In Case C, we saw that the biomass concentrations were low in the central eddy, but they were high inside the lobes. This is because the vertical exchange in the central eddy exceeds the critical value, whereas this critical value is not exceeded in the lobes. An even more striking example of an intermediate situation between

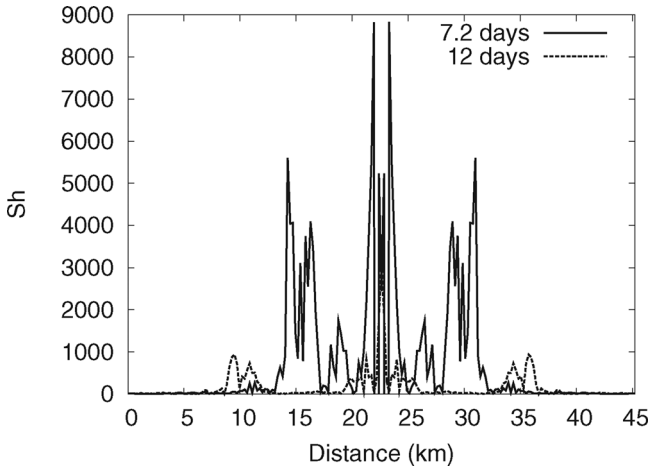

Figure 9. Sections (southwest-northeast through eddy centre) of the local Sherwood number as defined in Eq. 7 after 7.2 and 12 days at 20 m depth.

the two regimes is provided by Case D. After 7.2 days, the highest biomass concentrations are found outside the eddy and the lobes (Figs. 5a and b), whereas they are found within the lobes after 12 days (Fig. 5c). This can be explained from a change in the vertical transports with time, as we will show now.

A useful measure of the vertical transport by the flow is given by the Sherwood number (Sh). This dimensionless number is defined as the ratio of the total (i.e. diffusive plus advective) to the diffusive vertical nutrient flux:

$$Sh = \frac{\left| D_V \frac{\partial X_N}{\partial z} + w X_N \right|}{\left| D_V \frac{\partial X_N}{\partial z} \right|} \tag{7}$$

where the || denote the local absolute value. Because the diffusive transport is almost constant in our simulations, Sh is in fact a measure of the vertical advective mixing. As shown in Figure 9, Sh decreases dramatically between 7.2 and 12 days in the eddy and the lobes for Case D. From a one-dimensional water-column simulation, we have found that $D_{Vc} = 0.006$ m^2/s^{-1} for Case D. In the 3D model, this roughly corresponds to Sh = 600. This value is exceeded in most parts of the eddy region after 7.2 days, whereas after 12 days, Sh is almost nowhere above the critical value (see Fig. 9). Hence, the eddy region is initially in the light-limited regime and therefore, the plankton population only grows outside the eddy and the lobes. However, once the vertical exchange in the eddy and the lobes becomes lower than the critical turbulence, the phytoplankton population begins to grow in that region. After 12 days, the population in the lobes has grown so much that the maximum biomass concentration is found there.

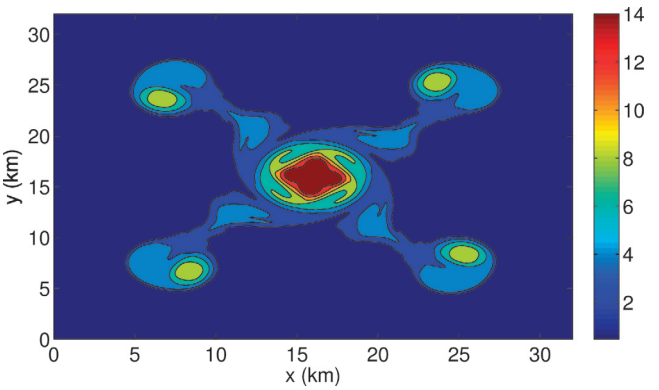

Figure 10. Surface distribution of a passive tracer after 12 days.

In Figures 6 and 7, we observe an asymmetry in the biomass distributions within the lobes after 12 days. If our three-dimensional version of the critical turbulence mechanism is also responsible for these small-scale distributions, then we expect that the locations with the highest vertical exchange correspond with biomass maxima, if the light intensity is high, and that these locations correspond with biomass minima, if the light intensity is low. Because the algae need time to grow, it is not only the instantaneous vertical exchange (or Sh) that is important, but also how much vertical exchange the algae have experienced in the past. One may solve this problem by considering the time development of the distribution of Sh within the lobes. However, it is not clear to what extent the positions of water masses relative to each other within the lobes remain the same. Therefore, we have chosen to use a passive tracer to determine the amount of vertical exchange that a water mass has experienced. At the start of the simulation, the horizontal distribution of this tracer is homogeneous and the tracer concentration increases monotonically in the vertical direction. Hence, locations with a high tracer concentration correspond with water masses that have experienced a relatively large vertical exchange. In Figure 10, we show the tracer distribution after 12 days. Comparing this tracer distribution with the biomass distributions, we see that the parts of the lobes that have experienced the largest vertical exchange (i.e. the front sides) correspond to biomass maxima in the simulation with the highest light intensity (Case A, see Fig. 3c) and to biomass minima in the simulations with lower light intensities (Cases B, C, and D, see Fig. 6). Hence, the asymmetries in the lobes can indeed be understood from local differences in the vertical exchange.

In the three-dimensional simulations, the regions with an elevated biomass concentration around the eddy turn out to be much broader than in the simulations with the idealised two-dimensional model. The reason for this difference seems not immediately obvious. In both types of simulations, the critical turbulence is exceeded inside the eddy, but the vertical exchange is far below the critical value everywhere outside the eddy. Furthermore, in both

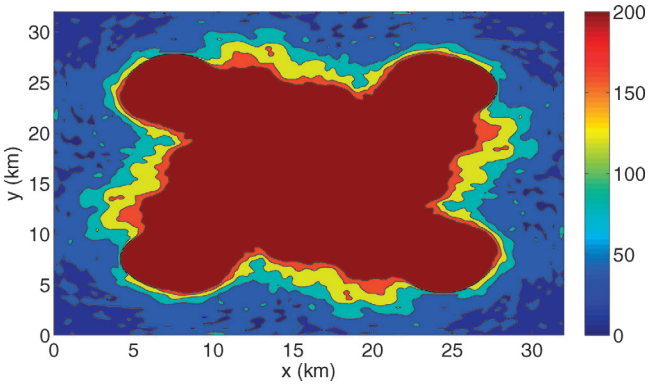

Figure 11. Surface distribution of the nutrient concentration X_N after 12 days for case C. Values are in nM.

types of simulations, the nutrient concentration is much higher adjacent to the eddy than in the regions farther away; this seems to make the region just adjacent to the eddy the optimal location for plankton growth. However, there is a subtle, but important difference in the nutrient distributions. In the 2D simulations, the nutrient concentration far away from the eddy remains practically the same during the first 12 days, whereas in the 3D simulations, the nutrient concentration far away from the eddy slightly increases. In a region extending quite far beyond the edges of the eddy and the lobes, the nutrient concentration is higher than 200 nM after 12 days (Fig. 11). In the regions far away from the eddy, the net growth rate remains practically equal to 0 in the 2D simulations (i.e. the growth and death rates remain approximately equal), whereas the net growth rate becomes positive in the 3D simulations. In Figure 12, we show a surface cross-section of the difference between a passive tracer with

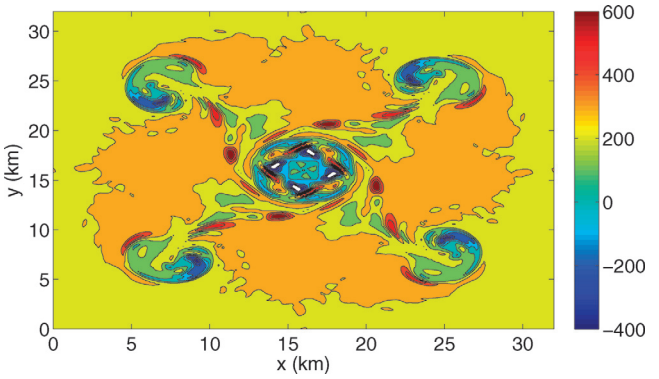

Figure 12. Surface distribution of a passive tracer minus the nutrient concentration X_N for case C after 12 days. Values are in nM. Hence, high positive values correspond with a large cumulative biotic nutrient consumption.

Table 5. Surface nutrient concentration X_N (nM) and biomass growth rate μ (d^{-1}) at the surface at x = 1.6 km, y = 16 km for the two- and three-dimensional simulations with surface light intensity $J_{L,S} = 2$ mol/(m^2d) at various times. The maximum biomass growth rate is equal to 0.185 d^{-1}.

		2D		3D	
		X_N	μ	X_N	μ
	0	5.4	0.102	5.4	0.102
	3.6	5.3	0.100	5.9	0.108
Time (d)	7.2	5.5	0.103	35	0.178
	12	5.6	0.104	70	0.183

initially the same distribution as the nutrient X_N and X_N itself for Case C after 12 days. This difference provides an indication of the cumulative biotic nutrient consumption. Broadly, it turns out to be high in the regions around the eddy and the lobes and low or even negative within the central eddy and the lobes. In those regions, the algal growth rate even approaches the maximum growth rate, as we show in Table 5, because the nutrient uptake saturates already at very low nutrient concentrations, if the light intensity is low. This implies that the plankton adjacent to the eddy can barely grow faster than the plankton far away from the eddy and therefore, the peak in plankton concentration adjacent to the eddy cannnot become very pronounced. The slight differences in nutrient distribution between the two- and three-dimensional simulations can be explained by a higher horizontal and vertical exchange in the region outside the eddy in the three-dimensional simulation. These higher transports are caused by various substructures in the flow (successive instabilities) that are absent in the 2D simulations.

5. Discussion and conclusions

We have investigated the impact of submesoscale vertical mixing on spatial distributions of plankton. The emerging distributions turn out to be strongly dependent on light and horizontal and vertical transports. In some cases, the highest biomass concentration is found in the eddy center, whereas in other cases, the maximum plankton concentration is in a region around the eddy. This can be understood from a three-dimensional analogue of the (one-dimensional) Huisman *et al.* (1999) critical turbulence concept. An eddy becomes rich in biomass, if the critical turbulence is not exceeded; in eddies where this critical (vertical) mixing is exceeded, the algae die out as a consequence of light limitation. The inclusion of horizontal exchange then has a crucial impact on the plankton distributions: the vertical exchange within the eddy transports nutrients to the surface which are dispersed into the region around the eddy. In that region, the conditions for plankton growth become optimal: a high nutrient concentration combined with a low downward transport of biomass.

Although we explain our main findings using the critical turbulence concept of Huisman *et al.* (1999), their 1D analogue does not capture all the relevant processes in our 3D world.

First of all, in our study, not only vertical exchange, but also horizontal transport plays a role in the explanation of the results. Another important distinction between the two studies is that we have investigated the transient behaviour of a plankton population in a strongly time-dependent flow field, whereas Huisman *et al.* (1999) studied the equilibrium distribution of plankton in a time-independent physical setting. As a consequence, the biomass concentration in Huisman *et al.* (1999) is equal to 0, if the critical turbulence is exceeded, whereas in our simulations, the biomass concentration will diminish at locations where the vertical mixing is above the critical value, but it does not become equal to 0. However, the main mechanism is essentially the same: competition between plankton growth and downward mixing of plankton out of the euphotic zone. If the growth exceeds the downward mixing, then the plankton concentration becomes higher, and if the growth cannot keep up with the mixing, then the plankton decreases.

In the vertical velocity fields (Fig. 2), small-scale features can be seen which may (partly) have a numerical origin. These small-scale features probably increase the vertical exchange which leads to an enhanced upward transport of nutrients and downward transport of biomass. Therefore, the model may overestimate these fluxes. Another possible source of inaccuracy may be the advection scheme for the biological tracers. It switches to a first-order upwind scheme (with a high numerical diffusion, Leonard and Mokhtari (1990)), if the gradients become very steep. Therefore, the smallest-scale variability in the biological tracers may be smoothed out.

Our biological model is highly idealised: a large number of potentially important factors were not included, e.g. cellular reserves, grazing, and self-shading. The different plankton patterns crucially depend on light- and nutrient-limitation. The inclusion of reserves would diminish the effects of both these limitations, because plankton with reserves can survive for some time under conditions of low light or low nutrients. Nevertheless, we also found influences of light- and nutrient-limitation on plankton patterns in Omta *et al.* (2007) where we simulated the same eddy as reported in the current article while using a plankton model with reserves. In these simulations, the biomass concentrations were low in the centre of the eddy (a consequence of light limitation) and in the region far away from the eddy (a consequence of nutrient limitation) whereas they were high at the edges of the eddy and the lobes.

An interesting effect is the impact of phytoplankton on the stratification of the water column (Sathyendranath *et al.* 1991; Morel and Antoine, 1994; Miller *et al.* 2003). By absorbing sunlight, algae heat the upper part of the water column which in turn leads to an increased stratification. Inclusion of this effect into our flow model would therefore lead to a lower vertical mixing, especially in the eddy region. Hence, the organisms would become light-limited at a lower light intensity and the boundary between the two main regimes would also shift to a lower light intensity.

Simulations of light-limited plankton growth in both a three-dimensional flow and a more idealized two-dimensional mixing layer model have been performed earlier by Fennel (2001). Both in these simulations and in our simulations at low light intensities, the biomass

concentrations became low in regions with deep vertical mixing. However, contrary to our results, Fennel (2001) did not find strips of high biomass adjacent to the regions of deep mixing. This difference can be explained, if we compare the two simulation setups. In our simulation, the surface nutrient concentration was very low, a typical situation for most of the world ocean. Under such circumstances, the plankton growth rate strongly increases with increasing surface nutrient concentration, as long as the critical turbulence is not exceeded. Hence, strips of high biomass concentrations were found adjacent to regions where the critical turbulence was exceeded, because the nutrient concentration was relatively high at those locations. In the Fennel (2001) simulation, the nutrient concentration was far above the saturation value for plankton everywhere in the domain, a situation that can be considered typical for continental shelf seas. Under such nutrient-replete conditions, the plankton growth rate does not depend on the nutrient concentration. In Fennel (2001), the plankton growth rate only depended on the mixing depth and therefore, the plankton concentrations became low in regions with deep mixing, whereas they became high in regions with shallow mixing.

Different studies with coupled flow-plankton models (Abraham, 1998; Spall and Richards, 2000) also suggest that plankton distributions can be very different from the upwelling patterns. In the explanations, however, the focus was on the delay between upwelling of nutrients and plankton growth. This effect always exists, regardless of whether the plankton is nutrient- or light-limited or not limited by anything at all (although the magnitude of the time delay does depend on limitation). The delay effect is relatively unimportant in our simulations, because we have taken the maximum plankton growth rate (μ_{max}) to be relatively high. Our results suggest that, apart from the delay effect, nutrient- and light-limitation can play an important part in the relationship between flow features and plankton distributions.

Unfortunately, satellite chlorophyll data are usually difficult to interpret at the sub-mesoscale because of the large number of interacting flow structures and biological processes. Therefore, it is difficult to test any model results describing effects of sub-mesoscale flow features on plankton distributions against observations. Nevertheless, we think that models could extend the interpretation of satellite chlorophyll data. It has, for example, been known from (satellite) observations for a long time that for some warm-core eddies, biomass concentrations are maximal in the centre, whereas for other warm-core eddies, biomass concentrations are highest at the boundaries of the eddy (Olson, 1986). According to our model results, such differences between eddies can be caused by differences in the vertical mixing and we hope that our study will therefore stimulate more detailed analysis of observed chlorophyll distributions.

Acknowledgments. We would like to thank George van Voorn, Jorn Bruggeman and three anonymous reviewers for careful reading and helpful comments and mark Van Raalte and Ben Sommeijer (CWI) for help with the numerics. This work was financially supported through the Computational Life Science program of the Netherlands Organisation for Scientific Research (NWO) under Grant No. 635.100.009.

REFERENCES

Abraham, E. R. 1998. The generation of plankton patchiness by turbulent stirring. Nature, *391*, 577–580.

Abraham, E. R., C. S. Law, P. W. Boyd, S. J. Lavender, M. T. Maldonado and A. R. Bowie. 2000. Importance of stirring in the development of an iron-fertilized phytoplankton bloom. Nature, *407*, 727–730.

Boyd, P. W., A. J. Watson, C. S. Law, E. R. Abraham, T. Trull, R. Murdoch, D. C. E. Bakker, A. R. Bowie, K. O. Buesseler, H. Chang, M. Charette, P. Croot, K. Downing, R. Frew, M. Gall, M. Hadfield, J. Hall, M. Harvey, G. Jameson, J. LaRoche, M. Liddicoat, R. Ling, M. T. Maldonado, R. M. McKay, S. Nodder, S. Pickmere, R. Pridmore, S. Rintoul, K. Safi, P. Sutton, R. Strzepek, K. Tanneberger, S. Turner, A. Waite and J. Zeldis. 2000. A mesoscale phytoplankton bloom in the polar Southern Ocean stimulated by iron fertilisation. Nature, *407*, 695–702.

Charney, J. G. 1947. The dynamics of long waves in a baroclinic westerly current. J. Meteor., *4*, 135–163.

Drijfhout, S. S. 2003. Why anticyclones can split. J. Phys. Oceanogr., *33*, 1579–1591.

Dubois, D. M. and Y. Adam. 1976. Spatial structuration of diffusive prey-predator biological populations: simulation of the horizontal distribution of plankton in the North Sea, *in* System Simulation in Water Resources, G. C. Vansteenkiste, ed., Amsterdam. North Holland, 343–356.

Eady, E. T. 1949. Long waves and cyclone waves. Tellus, *1*, 258–277.

Fennel, K. 2001. The generation of phytoplankton patchiness by mesoscale current patterns. Ocean Dyn., *52*, 58–70.

Flierl, G. R. and C. S. Davis. 1993. Biological effects of Gulf Stream meandering. J. Mar. Res., *51*, 529–560.

Flierl, G. and D. J. McGillicuddy. 2002. Mesoscale and submesoscale physical-biological interactions, *in* The Sea (12), A. R. Robinson, J. J. McCarthy, and B. J. Rothschild, eds, Wiley, New York.

Hardy, A. C. 1936. The continuous plankton recorder. Discovery Reports, *11*, 457–510.

Huisman, J., P. van Oostveen and F. J. Weissing. 1999. Critical depth and critical turbulence: Two different mechanisms for the development of phytoplankton blooms. Limnol. Oceanogr., *44*, 1781–1787.

Hundsdorfer, W. and J. G. Verwer. 2003. Numerical Solution of Time-Dependent Advection-Diffusion-Reaction Equations, Springer Verlag, Berlin, 1st edition.

Kierstead, H. and L. B. Slobodkin. 1953. The size of water masses containing plankton blooms. J. Mar. Res., *12*, 141–147.

Kooijman, S. A. L. M. 2000. Dynamic Energy and Mass Budgets in Biological Systems, Cambridge University Press, Cambridge.

Kooijman, S. A. L. M., H. A. Dijkstra and B. W. Kooi. 2002. Light–induced mass turnover in a mono–species community of mixotrophs. J. Theoretical Biol., *214*, 233–254.

Legg, S., J. McWilliams and J. Gao. 1998. Localization of deep convection by a mesoscale eddy. J. Phys. Oceanogr., *28*, 944–970.

Leonard, B. P. and S. Mokhtari. 1990. Beyond first-order upwinding: the ultra-sharp alternative for non-oscillatory steady-state simulation of convection. Intl. J. Num. Methods in Eng., *30*, 729–766.

Levin, S. A. and L. A. Segel. 1976. Hypothesis for the origin of plankton patchiness. Nature, *259*, 659.

Lévy, M. 2003. Mesoscale variability of phytoplankton and of new production: Impact of the large-scale nutrient distribution. J. Geophy. Res., *108*, 22.

Lévy, M., P. Klein and A. M. Treguier. 2001. Impacts of sub-mesoscale physics on phytoplankton production and subduction. J. Mar. Res., *59*, 535–565.

Martin, A. P. 2003. Phytoplankton patchiness: the role of lateral stirring and mixing. Prog. Oceanogr., *57*, 125–174.

McGillicuddy, D. J. and A. R. Robinson. 1997. Eddy-induced nutrient supply and new production in the Sargasso Sea. Deep-Sea Res. I, *44*, 1359–1398.

McGillicuddy, D. J., A. R. Robinson and J. J. McCarthy. 1995. Coupled physical and biological modeling of the spring bloom in the North Atlantic: (II) three-dimensional bloom and post-bloom effects. Deep-Sea Res. I, *42*, 1359–1398.

McGillicuddy, D. J., A. R. Robinson, D. A. Siegel, H. W. Jannasch, R. Johnson, T. D. Dickey, J. McNeil, A. F. Michaels and A. H. Knap. 1998. Influence of mesoscale eddies on new production in the Sargasso Sea. Nature, *394*, 263–266.

Miller, A. J., M. A. Alexander, G. J. Boer, F. Chai, K. Denman, R. Frouin, A. J. Gabric, E. A. Laws, M. R. Lewis, Z. Liu, R. Murtugudde, S. Nakamoto, D. J. Neilson, J. R. Norris, J. C. Ohlmann, R. I. Perry, N. Schneider, K. M. Shell and A. Timmermann. 2003. Potential feedbacks between pacific ocean ecosystems and interdecadal climate variations. Bull. Amer. Meteor. Soc., *84*, 617–633.

Molemaker, M. J. and H. A. Dijkstra. 2000. Stability of a cold–core eddy in the presence of convection: hydrostatic versus nonhydrostatic modeling. J. Phys. Oceanogr., *30*, 475–494.

Morel, A. and D. Antoine. 1994. Heating rate within the upper ocean in relation to its bio–optical state. J. Phys. Oceanogr., *24*, 1652–1665.

Niiler, P. P. 1969. On the Ekman divergence in an oceanic jet. J. Geophys. Res., *74*, 7048–7056.

Noh, Y., W. G. Cheon and S. Raasch. 2003. The role of preconditioning in the evolution of open-ocean deep convection. J. Phys. Oceanogr., *33*, 1145–1166.

Olson, D. B. 1986. Lateral exchange within gulf stream warm-core ring surface layers. Deep-Sea Res., *33*, 1691–1704.

Omta, A. W., J. Bruggeman, S. A. L. M. Kooijman and H. A. Dijkstra. 2006. The biological carbon pump revisited: feedback mechanisms between climate and the redfield ratio. Geophys. Res. Lett., *33*, L14613, doi: 10.1029/2006 GL026313.

Omta, A. W., S. A. L. M. Kooijman and H. A. Dijkstra. 2007. The influence of (sub-)mesoscale eddies on the soft-tissue carbon pump. J. Geophys. Res. Oceans, *112*, C11009, doi: 10.1029/2007 JC004189.

Petrovskii, S. V. 1999. On the plankton front waves accelerated by marine turbulence. J. Mar. Sys., *21*, 179–188.

Petrovskii, S. V. and H. Malchow. 1999. A minimal model of pattern formation in a prey-predator system. Math. Comp. Model., *29*, 49–63.

——— 2001. Wave of chaos: new mechanism of pattern formation in spatio-temporal population dynamics. Theor. Pop. Biol., *59*, 157–174.

Rothschild, B. J. and J. S. Ault. 1996. Population-dynamic instability as a cause of patch structure. Ecol. Model., *93*, 237–249.

Sathyendranath, S., A. D. Gouveia, S. R. Shetye, P. Ravindran and T. Platt. 1991. Biological control of surface temperature in the arabian sea. Nature, *349*, 54–56.

Seuront, L., F. Schmitt, Y. Lagadeuc, D. Schertzer, S. Lovejoy and S. Frontier. 1996. Multifractal analysis of phytoplankton biomass and temperature in the ocean. Geophys. Res. Lett., *23*, 3591–3594.

Seuront, L., F. Schmitt, Y. Lagadeuc, D. Schertzer and S. Lovejoy. 1999. Universal multifractal analysis as a tool to characterize multiscale intermittent patterns: example of phytoplankton distribution in turbulent coastal waters. J. Plank. Res., *21*, 877–922.

Skellam, J. G. 1951. Random dispersal in theoretical populations. Biometrika, *38*, 196–218.

Smith, R. C., X. Zhang and J. Michaelsen. 1988. Variability of pigment biomass in the california current system as determined by satellite imagery. 1. spatial variability. J. Geophys. Res., *93*, 10863–10882.

Spall, S. A. and K. J. Richards. 2000. A numerical model of mesoscale frontal instabilities and plankton dynamics: I. model formulation and initial experiments. Deep-Sea Res. I, *47*, 1261–1301.

Stern, M. E. 1965. Interaction of a uniform wind stress with a geostrophic vortex. Deep-Sea Res., *12*, 355–367.

Strass, V. H. 1992. Chlorophyll patchiness caused by mesoscale upwelling at fronts. Deep-Sea Res. A, *39*, 75–96.

Sverdrup, H. U. 1953. On conditions of the vernal blooming of phytoplankton. J. Conseil International Pour l'exploration de la mer, *18*, 287–295.

Tél, T., A. de Moura, C. Grebogi and G. Károlyi. 2005. Chemical and biological activity in open flows: A dynamical system approach. Physics Rep., *413*, 91–196.

Turing, A. M. 1952. The chemical basis of morphogenesis. Phil. Trans. Roy. Soc. London B, *237*, 37–72.

Woods, J. 1988. Mesoscale upwelling and primary production, in Toward a Theory on Biological-Physical Interactions in the World Ocean, B. Rothschild, ed., Dordrecht. D. Reidel.

Received: *25 June, 2007*; revised: *21 January, 2008*.